Upregulation of COX4-2 *via* HIF-1α in mitochondrial COX4-1deficiency

Liza Douiev[1*], Chaya Miller[1], Shmuel Ruppo[2], Hadar Benyamini[2], Bassam Abu-Libdeh[3], Ann Saada[1,4*]

Affiliations

[1] Department of Genetics, Hadassah Medical Center, Jerusalem 9112001, Israel.
[2] Info-CORE, I-CORE Bioinformatics Unit of the Hebrew University of Jerusalem and Hadassah Medical Center
[3] Department of Pediatrics, Makassed Hospital and Al-Quds University, Jerusalem 91220, Palestinian Authority
[4]Faculty of Medicine, Hebrew University of Jerusalem, 9112001, Israel

*corresponding authors

Prof. Ann Saada (Reisch), Department of Genetics, Hadassah Medical Center, Jerusalem 9112001, Israel. annsr@hadassah.org.il, anns@ekmd.huji.ac.il

Liza Douiev, Department of Genetics, Hadassah Medical Center, Jerusalem 9112001, Israel liza.douiev@mail.huji.ac.il

Abstract

Cytochrome-*c*-oxidase (COX) subunit 4 (COX4) plays important roles in the function, assembly and regulation of COX (mitochondrial respiratory complex 4), the terminal electron acceptor of the oxidative phosphorylation (OXPHOS) system. The principal COX4 isoform, COX4-1, is expressed in all tissues, whereas COX4-2 is mainly expressed in the lungs, or under hypoxia and other stress conditions. We have previously described a patient with a COX4-1 defect with a relatively mild presentation compared to other primary COX deficiencies, and hypothesized that this could be the result of compensatory upregulation of COX4-2. To this end, COX4-1 was downregulated by shRNAs in human foreskin fibroblasts (HFF), and compared to patient's cells. COX4-1, COX4-2 and HIF-1α were detected by immunocytochemistry. The mRNA transcripts of both COX4 isoforms and HIF-1 target genes were carried out by RT-qPCR. COX activity and OXPHOS function were measured by enzymatic and oxygen consumption assays, respectively. Pathways were analyzed by CEL-Seq2 and by RT-qPCR.
We demonstrate elevated COX4-2 levels in the COX4-1-deficient cells with a concomitant HIF-1α stabilization, nuclear localization and upregulated hypoxia and glycolysis pathways. We suggest that COX4-2 and HIF-1α has the are upregulated, also in normoxia as a compensatory mechanism in COX4-1 deficiency.

Key Words
Mitochondria, cytochrome *c* oxidase, COX4-1, COX4-2, HIF-1α

1. Introduction:

The mammalian cytochrome *c* oxidase (COX, mitochondrial respiratory chain complex IV) is a dimeric multi-subunit complex which is comprised of fourteen mitochondrial and nuclear-encoded subunits. COX is considered the rate-limiting complex of the oxidative phosphorylation system (OXPHOS). The two unique regulatory mechanisms (compared to the other OXPHOS complexes) are; the expression of isoforms and the binding of specific regulatory factors to nuclear-encoded subunits [2 Arnold. *Mitochondrion.* 2012]. One important regulatory mechanism involves the COX4 isoforms and feedback inhibition by ATP. COX4 is the largest nuclear encoded subunit and plays important roles in COX function, assembly and regulation. It is allosterically inhibited at high ATP/ADP ratios, and by phosphorylation, allowing fine tuning of the mitochondrial respiratory capacity. COX4 isoform 1 (COX4-1), which is the main subunit 4 of COX, is ubiquitously expressed in mammalian tissues under normoxic conditions. COX4 isoform 2 (COX4-2) the less common isoform, is primarily expressed in the lung and in lower levels in the placenta, heart, brain and pancreas. COX4-2 is preferentially expressed under hypoxia and oxidative stress and it is suggested that the isoform switch results in a more efficient COX activity. [2 Arnold, 3 Timon].

In 2017, we reported a novel form of COX deficiency caused by a K101N variant in *COX4I1* gene encoding COX4-1 in a patient presented with Fanconi anemia-like features, short stature and mild dysmorphism, while all known Fanconi Anemia (FA) gene sequences were intact. We proved the pathogenicity of the homozygous K101N variant by demonstrating 25% residual COX activity in patients' fibroblasts homogenate, almost undetectable COX4-1 protein in mitochondria, and by performing complementation studies with the wild-type gene [4Abu-Libdeh, 2017]. Additionally, we verified chromosomal instability by Phospho-Histone H2A.X (γH2AX) staining [5 Douiev 2018]. Recently, an additional pathogenic COX*4I1* variant (P152T), associated with a much more severe phenotype resembling Leigh syndrome with developmental regression abnormal MRI and 16% residual COX activity in muscle, was reported by Pilali et al. [6 Pilali].

Notably, the phenotype in our patient was different and relatively mild compared to the COX4-1 P152T patient and other patients with isolated COX deficiencies, and nuclear-encoded mitochondrial diseases in general [7 RAK, 8 shoubridge,9Hock 2020]. Accordingly, we hypothesized that a compensatory isoform switching to COX4-2 is able to, at least partially, compensate for the deficient COX4-1. In this work, we demonstrate elevated COX4-2 in the K101N patient's fibroblasts as well as in a human foreskin fibroblasts cell line (HFF) with stable COX4-1 knockdown. This upregulation is linked to HIF-1α stabilization, nuclear localization and upregulation of both hypoxia and glycolysis pathways.

2. Materials and Methods:

2.1. Tissue cultures

Previously established skin primary fibroblasts cultures from the patient (Informed consent was obtained IRB #0485-09) [4Abu-Libdeh 2017] controls and human foreskin fibroblasts (HFF-1 ATCC) were maintained in high-glucose DMEM supplemented with 15% fetal bovine serum, L-glutamine, pyruvate and 50μg/mL uridine (Biological Industries, Beit Ha'emek, Israel). For immunocytochemistry, cells were seeded on u-slide 8 well-ibiTreat sterile tissue culture slides (NBT; New Biotechnology Ltd., Jerusalem, Israel). For western blot or RNA analysis, cells were seeded, cells were grown in tissue culture bottles. For positive hypoxia controls in (Immunostaining and western blot) cells were pre-incubated with 500μL $CoCl_2$ supplemented within a new fresh media, for 6 or 24 hours, at 37°C, 5% CO_2 [10 Shteyer2009]. All cells were incubated at 37 °C in a humidified 5% CO_2 atmosphere.

2.2. RNA interference

For the downregulation of *COX4I1*, we employed the MISSION® shRNA plasmid DNA vector system. The system included five plasmids each is targeted against different site of *COX4I1*. In addition, we used a non-mammalian shRNA Control Plasmid DNA target as a control vector (Sigma-Aldrich). We introduced each of the DNA plasmids into HEK293FT cells by co-transfection with pLP1, pLP2, and pLP/VSVG plasmids using lipofectamine (ViraPower; Invitrogen, California, USA). Human foreskin fibroblasts were infected with viral supernatant containing polybrene. Stably transfected cells were selected with puromycin (2μg/mL) for three-weeks. Preliminary results showed that shRNA #TRCN0000232554 (COX4-1 shRNA) was the most suitable.

2.3. Quantitative reverse transcription polymerase chain reaction (RT-qPCR)

Total RNA was isolated from patient, HFF-shRNA, HFF-CV and healthy control primary fibroblasts with Tri-Reagent (Telron, Isarel) and cDNA from poly(A)+mRNA was generated using Improm II, Promega, Madison, WI, USA. Real time, quantitative PCR for the quantification of COX4I1, COX4I2, PDK1, SLC2A1, HK1, HK2, GUSB and GAPDH transcripts - was performed using Fast SYBR GreenMaster Mix and the ABI PRISM7900HT sequence detection system (Applied Biosystems, Foster City, CA, USA). The following primer sequences were used fo qPCR:

Gene	Forward primer	Reverse primer
COX4I1 (NM_001861.6)	5'-TTTCACCGCGCTCGTTAT-3'	5'-CTTCATGTCCAGCATCCTCTT-3'
COX4I2 (NM_032609)	5'-GAAGACGAGGGATGCACAG-3'	5'-GGCTCTTCTGGCATGGG-3'
PDK1 (NM_001278549.2)	5'- CAGGACACCATCCGTTCAAT-3'	5'- AGCTTTAGCATCCTCAGCAC-3'
GLUT1 (NM_006516.4)	5'-GCTACAACACTGGAGTCATCAA-3'	5'-ACTGAGAGGGACCAGAGC-3'
HK1 (NM_000188.3)	5'- CCCTAAATGCTGGGAAACAAAG-3'	5'- CCCTTCTTGGTGAAGTCGATTA-3'
HK2 (NM_000189.5)	5'- CATCCTCCTCAAGTGGACAAA-3'	5'- ACCACATCCAGGTCAAACTC-3'
GUSB (NM_000181.4)	5'-GAAAATATGTGGTTGGAGAGCTCATT-3'	5'-CCGAGTGAAGATCCCCTTTTTA-3'
GAPDH (NM_001357943.2)	5'-CAAGAGCACAAGAGGAAGAGAG-3'	5'-CTACATGGCAACTGTGAGGAG-3'

2.4. COX enzymatic activity

COX activity in cells disrupted by sonication and solubilization with 0.5mg/mL -dodecyl-β-D-maltoside (Calbiochem, San-Diego, CA, US) on ice, was determined by spectrophotometry monitoring the oxidation of 50μM reduced cytochrome *c* at 550nm in 10mM potassium phosphate buffer, pH7.0 at 37°C on a Kontron UVICON xs double beam spectrophotometer (Secomam, France)

2.5. Oxygen Consumption rate

Oxygen consumption rate (OCR) was measured using Agilent Seahorse XF Cell Mito Stress Test Kit (#103015-100) (Seahorse Biosciences, North Billeric, MA, USA). 10,000 cells/well were seeded on an XF96-well plate. Following 72 hr, the growth medium was changed to an unbuffered DMEM (Agilent Technologies, Inc. Wilmington, USA) supplemented with 10mM glucose 1mM pyruvate and 2mM glutamine and the plate was equilibrated at 37°C for 1 hr before the measurements. In the absence and in the presence of sequentially added 2.5 μM Oligomycin, 2 μM Carbonyl cyanide-4 (trifluoromethoxy) phenylhydrazone (FCCP), 0.5 μM Rotenone and Antimycin), according to the manufacturer's instructions. Oxygen consumption rate (OCR) and extra cellular acidification rate ECAR, were calculated relative to cell content per well, estimated by the methylene blue assay which is proportional to cell count, as we have previously described [11Golubitzky]. Briefly, cells were fixed with 0.5% glutaraldehyde for 10 min, rinsed with double-distilled water, stained with 1% methylene blue in 0.1M borate buffer pH 8.5 for 1 hr, rinsed with water, and allowed to dry. The dye was extracted from the cells with 0.1N HCl at 37°C for 1 hr, then measured at A620 nm.

2.6. Immunofluorescence staining

The cells were seeded on u-slide 8 well-ibi-Treat sterile tissue culture slides. On the following day, the media was replaced by a fresh media in the presence or absence of cobalt. Following 6 hr of incubation, the cells were fixed with 4% paraformaldehyde for 15 min at room temperature, and then permeabilized with either 0.3% (HIF-1 and COX4-2 staining) or 0.2% (COX4 isoform staining) Triton X-100. After blocking with 1% BSA /PBS for 1 hr at room temperature, slides were incubated with primary antibody at 4℃ overnight. On following day, the cells were washed 3 times with PBS, and incubated with fluorescence-conjugated secondary antibodies for 1 hr at room temperature in dark. The following primary antibodies were used for immunofluorescence: HIF-1α (1:500; GTX127309 GeneTex Inc, Irvine, CA USA,), COX4-1 (1:150; 6431 MitoSciences, USA A-Molecular Probes, Eugene,Oregon,USA) and COX4-2 (1:150; H00084701-M01, Abnova,Taipei,Taiwan).Secondary antibodies: anti-Rabbit Cy5 (711-175-152) and anti-mouse DyLight 488 (115-485-062) (both from Jackson Immuno research, Laboratories, Baltimore Pike,PA,USA).The slides were subsequently washed 3 times with PBS and nuclei were stained with Hoechst 33342, NucBlue live cell stain (Molecular probes, Life technologies Eugene OR, USA). Mitochondria were visualized using MitoTracker Red CM-H2XRos (MTR) (Molecular probes, Life technologies Eugene OR, USA). In brief, cells were incubated with 2μM MTR for 30 min, at 37°C, 5% CO_2. Then, the cells were washed with PBS and incubated with a fresh high-glucose media for another 45 min (in the dark). The cells subsequently were fixed as mentioned above. The cells were examined by fluorescence confocal microscopy, X60 or X40 magnifications (Nikon A1R). Image analyses were performed by the quantification of fluorescence signals per nuclei (HIF-1α) or per cell (COX4 isoforms) using the Image J software http://imagej.nih.gov/ij (National Institute of Health, Bethesda, MD, USA)

2.7. Western blot

Western blot assay (WB) was performed using the BIO-RAD kit. The samples were prepared as follows: the cells were washed with ice-cold PBS, harvested on ice, and immedicately incubated in Laemmli sample buffer 95ºC for 5 min.. Subsequently, the samples were subjected to SDS-PAGE (Mini-protean, any-kD precast gel), transferred to PVDF membrane, and blocked with Every Blot Blocking Buffer according to the manufacturer's instructions (Bio-Rad, Hercules, CA, USA). The membrane was incubated with rabbit anti HIF-1α antibodies (GenTex, CA, USA; Cat#: GTX127309) (1:1000), overnight, at 4°C. The following day, membranes were washed with TBS-Tween and incubated with peroxidase-conjugated donkey anti rabbit (Jackson Immuno Research laboratories, West Grove, PA, USA; Cat#:111-035-144) for 1 hr, at RT. Membranes were visualized with enhanced Clarity Max ECL detection (Bio-Rad), and were detected with the Fusion Solo system (Vilber Lourmat). Thereafter the membranes were washed and then incubated with mouse monoclonal antibody against actin (1:500; Cat#: 691001, MP Biomedicals, Ohio, USA) for 2 hr, at RT, washed and incubated peroxidase-conjugated goat-anti mouse antibody (Cat#:115-035-062, Jackson Immuno Research laboratories, West Grove, PA, USA;) for 1 hr, at RT and visualized as above. Band intensities were measured by imageJ http://imagej.nih.gov/ij (National Institute of Health, Bethesda, MD, USA).

2.8. Expression by Linear Amplification and Sequencing: CEL-Seq2

Total RNA was isolated from COX4-1 shRNA transfected cells or control HFF. Qualification and quantification were measured using Tapestation. A HiSeq assay using CEL-Seq2 method [12 Hashimshony] was performed at the Technion Genome Center, Haifa Israel. Briefly, 3′ cDNA was synthesized and barcoded, followed by RNA synthesis and amplification by in vitro transcription.

Statistic and bioinformatic analysis of the CEL-Seq2 data was performed in collaboration with the Info-CORE Bioinformatics Unit (Hebrew University of Jerusalem and Hadassah Medical Center). Following demultiplexing, reads were quality filtered and

trimmed for adapters as well as for poly-A tails using Cutadapt [13 Marcel]. Then they were aligned to the human genome (GRCh38 with annotations from Ensembl release 95) using Tophat v2.1.1 [25 Kim], and quantified with HTSeq [14 Anders].

Differential expression analysis was done with the DESeq2 package (v1.22.1) [27 Love]. Genes with a sum of counts less than 10 over all samples were filtered out. Differential expression was calculated with default parameters except not using the independent Filtering algorithm. Significance threshold was set as FDR<0.1.

Visualization was performed using Glimma (1.10.1) [28 Su]. Results were combined with gene details (such as symbol, known transcripts, etc.), taken from the results of a BioMart query (Ensembl, release 95), to produce the final Excel file. In order to identify biological functions that were expected to be influenced (either to increase/ decrease) given the observed gene expression changes (between HFF-shCOX4I1 and healthy control fibroblasts), we ran gene set enrichment analysis (GSEA, reference: https://www.ncbi.nlm.nih.gov/pmc/articles/PMC1239896/). GSEA uses whole differential expression data (cut-off independent) to determine whether a priori–defined sets of genes show statistically significant, concordant differences between two biological states. We used the hallmark gene set collection from the molecular signatures database (MsigDB). Expression Data results are in the process of uploading on the GEO (Gene expression Omnibus) website (https://www.ncbi.nlm.nih.gov/geo/).

2.9. Statistical analysis

Statistical analysis was done by two tailed-student's unpaired *t*-test using IBM SPSS statistics for Windows, version 24.0. software (IBM Corp. Armonk, NY, USA). p values < 0.05 were considered statistically significant.

3. Results:

3.1. COX4 isoform switch and altered energetic profile in COX4-1-deficient cells.

In order to characterize COX4-1 deficiency in HFF-shCOX4I1 and in patient's cells we initially quantified *COX4I1* mRNA transcripts by RT-qPCR and detected a significant 86% and 60% decrease relative to controls respectively. This verified our previous preliminary findings in the patient's cells and the efficacy of the shRNA which downregulated, but not depleted *COX4I1* expression. Reciprocally COX4I2 transcripts were elevated x1.72 times in the HFF-shCOX4I1 cells and even more so (x16 times) in patients' cells (Fig. 1A,B). Enzymatic activity of COX was, as expected, significantly reduced, but not abolished, in both HFF-shCOX4I1 and the patients' cells (80-45% decrease respectively) (Fig. 1C,D), relative to corresponding controls. To address whether the isoform switch translates into a change in allosteric properties as was previously reported by Arnold and Kadenbach [15]we measured COX activity in isolated mitochondrial in the presence of 10mM ATP. The COX activity (31 nmol/min/mg) in patients' fibroblasts mitochondrial was not affected by ATP, while mitochondria that were isolated from control fibroblasts showed a significant 52% inhibition upon preincubation with ATP (115±39 nmol/min/mg and 55±13 nmol/min/mg, respectively). Regretfully, we could not repeat this experiment in the HFF-shCOX4I1 cells because of impaired cell growth (manuscript in preparation) which hindered mitochondrial isolation.

We also monitored both the mitochondrial respiration (indicated as the oxygen consumption rate; OCR) and the glycolysis (estimated by the extracellular acidification rate (ECAR) of the surrounding media) (Fig.1E-J). Maximal OCR reflects the maximal respiratory capacity following the addition of the uncoupler FCCP. We calculated the ATP-linked respiration, by subtracting the OCR values obtained following the addition of oligomycin (an ATP synthase inhibitor) from the basal OCR (Fig.1G,H). The background, oxygen consumption, in the presence of the respiratory chain inhibitors rotenone and antimycin were subtracted from the OCR values and all values were normalized to cell content.

When comparing HFF-shCOX4I1 cells and the patients' cells relative to their corresponding controls we clearly detected different energetic profiles (Fig. 1I,H). Basal and maximal OCR and ATP dependent OCRs in the HFF-shCOX4I1 cells were decreased by 30%-40%, but to a lesser extent than expected from the *COX4I1* transcripts (Fig. 1A,B). The OCRs were even less affected in the patient's cells (Fig. 1E,F). Nevertheless, the energy maps, combining decreased basal OCR with increased ECAR, clearly showed a tendency of favoring glycolysis over OXPHOS in both the HFF-shCOX4I1 and somewhat less pronounced in the patient's cells (Fig. 1I-J).

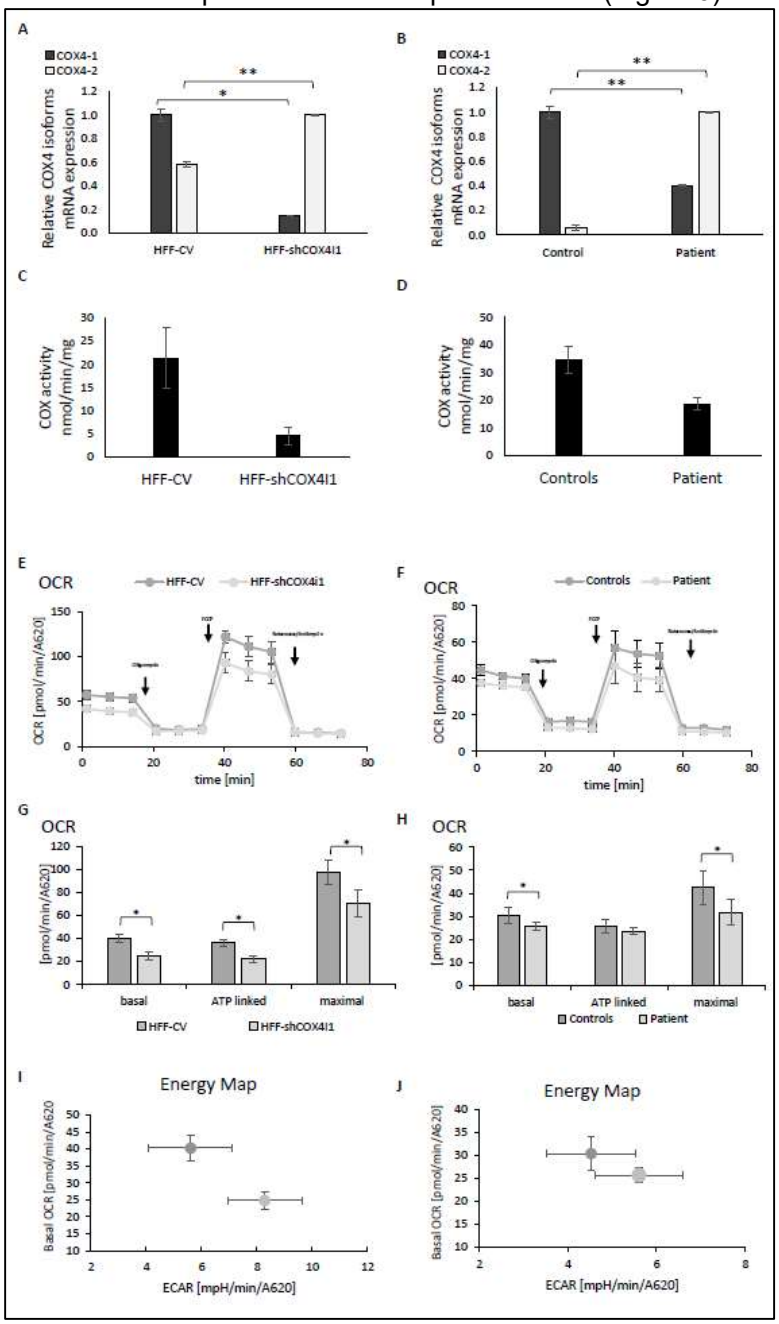

Figure 1. Decreased COX4I1 expression, COX activity and mitochondrial respiration with elevated glycolysis trend in COX4-1-deficient cells. mRNA expression levels of COX4 isoforms were measured by RT-qPCR in the knockdown vs. control cell lines (COX4-1 knockdown was obtained using a stable expression of COX4I1-targeting or non-mammalian target shRNAs, respectively) (A) and in patients' and healthy controls

fibroblasts (B). The results revealed decreased levels of COX4I1 mRNA expression and a reciprocally elevated levels of COX4I2 mRNA expression in both COX4-1-deficient cells. Enzymatic activity of COX determined by spectrophotometry, shows decreased activity (C&D) both in shCOX4I1 and patients' cells, relative to corresponding control. Oxygen consumption rate (OCR) and extracellular acidification rate; ECAR were measured in shCOX4I1 (E,G,I) and patient cells (F,H,J) and in corresponding controls, with subsequent addition of Oligomycin, FCCP and Antimycin/Rotenone. Basal, ATP-linked and maximal OCR were calculated (G,H) and OCR was plotted against ECAR to construct energy maps (I,J). All values were normalized to cell content measured by methylene blue (A620). OCR was reduced, relative to the corresponding controls. Both COX4-1-deficient cell lines showed a tendency towards glycolysis than the corresponding controls. Values are presented as normalized mean± SEM; *p<0.05; **p<0.01 compared to corresponding control.

The relative mild decrease of both OCR and COX activity in the patients' cells and the significant residual OCR and COX activity in the HFF-shCOX4I1 cells could possibly be explained by compensating upregulation of *COX4I2* expression as we observed by RT-qPCR. Therefore, for verification we analyzed the presence of the COX4-2 protein by immunofluorescence. As depicted in Figure 2 A-B, COX4-1-deficient cells indeed showed a significant reduction in the COX4-1 protein, while displaying significant reciprocal elevation in COX4-2 protein, in accord with our assumption. (Regretfully, in our hands, the anti-COX4-2 antibodies were not suitable for immunoblot in cell homogenates).

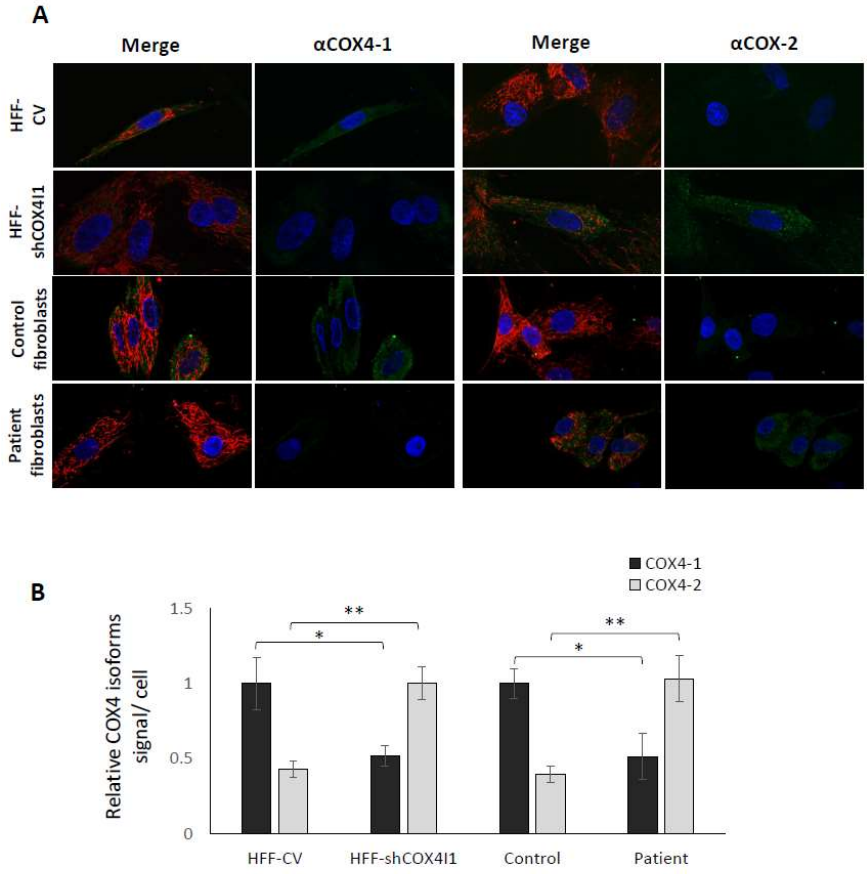

Figure 2. Decreased COX4-1 with a reciprocal elevation of COX4-2 in COX4-1-deficient cells. Knockdown (HFF-shCOX4I1), patients' and corresponding control cells were incubated with mitotracker red, fixed and stained separately with antibodies against COX4-1 and COX4-2. The results displayed in A&B demonstrate markedly decreased COX4-1 levels in both COX4-1-deficient cells (HFF-shCOX4I1 and patients' cells), while COX4-2 staining is increased, relative to respective controls. Nuclei were visualized with Hoechst-33342 (A). The micrographs were quantified and depicted as histograms of signal intensity per cell ± SEM of at least 100 cells *0.05<p; **0.01<p (B).

3.2. Upregulation of glycolytic and hypoxia pathways in COX4-1-deficient cells

COX4 isoform 2 is mainly expressed in the lungs, and at low levels in the placenta, heart, brain and pancreas. COX4 isoform 2 gene (*COX4I2*) is featured with an oxygen responsive element (ORE), which is HIF-1-independent. COX4-2 expression is controlled by, at least, two mechanisms. That is either through the regulation of HIF-1 or *via* its ORE where transcription is regulated by the interplay of three regulatory transcription factors: RBPJ, CXXC5 and CHCHD2 [16Aras 2014]. In order to identify the possible pathways that regulate the observed isoform switch, we performed CEL-Seq2 analysis HFF-shCOX4I1 and compared the RNA expression pattern with the HFF control (with the same genetic background) from five RNA extractions performed on different occasions. The main significantly upregulated pathways were epithelial mesenchymal transition (EMT), glycolysis and hypoxia (Figure 3A), (A list of up regulated genes is available in the supplementary table). The upregulation of glycolysis was in accord with the previously mentioned energy map showing decreased OCR with elevated ECAR. However, the pathway that caught our attention was hypoxia and among the potential mediators of hypoxia-induced EMT is the hypoxia-inducible factor-1α (HIF-1α), which is a transcription factor [17Tam et al 2020] linked among many other functions, also to the upregulation of COX4-2 under hypoxia [18Fukuda]. In order to validate these results, and to confirm the involvement of the HIF-1α pathway we performed RT-qPCR validations, to detect and quantify the levels of several major HIF-1 target genes. As represented in Figure 3-C, we verified the upregulation of four HIF-1α target genes (including: PDK1, GLUT1, HK1 and HK2) observed in CEL-Seq2 (represented in the volcano plot: Figure 3B) which were also up-regulated in both knock-down and in the patient's fibroblasts.

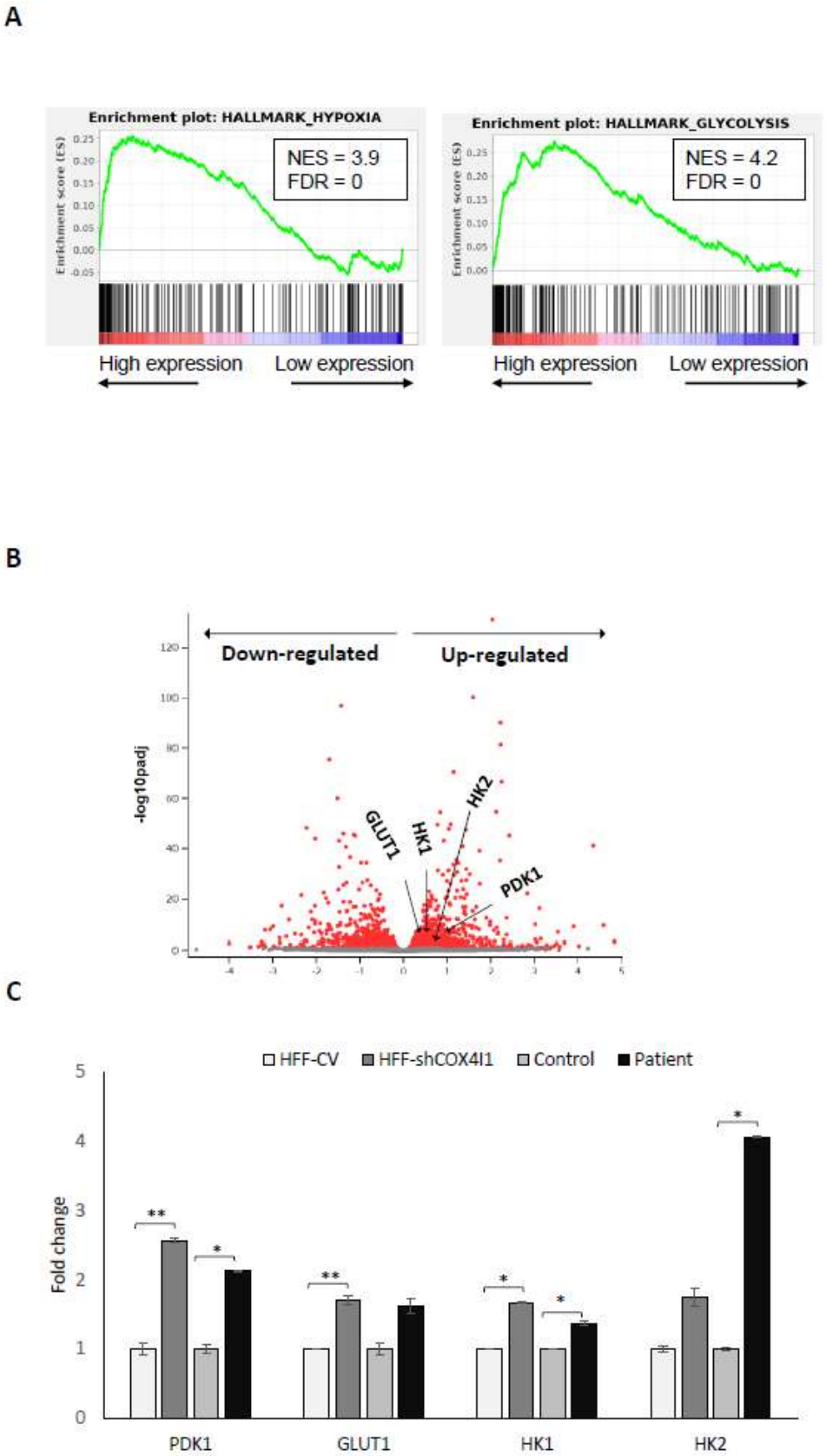

Figure 3. CEL-Seq2 analysis identified hypoxia as one of the top up-regulated pathways in COX4-1-deficient cells. Total RNA was isolated from both COX4-1-deficient cells (HFF-shCOX4I1 and patient)

and from both types of control cells (HFF-CV and healthy control fibroblasts). A HiSeq assay was performed at the Technion Genome Center using the CEL-Seq2 method. Differential expression analysis was done with the DESeq2 package. Significance threshold was set as FDR<0.1. In order to identify biological functions that were expected to be influenced (either to increase/ decrease) given the observed gene expression changes (between HFF-shCOX4I1 and the healthy control fibroblasts), Pathway Analysis was subsequently performed. Up-regulation of hypoxia (left) and glycolysis (right) detected by GSEA (reference). NES: normalized enrichment signal; FDR: false discovery rate (A). In the volcano plot, each dot represents a gene (B). The x-axis indicates the log2 (Fold Change) of the expression of HFF-shCOX4I1 relative to healthy control fibroblasts, and the y-axis reflects –log10 of the FDR adjusted p-value of this comparison. The colored dots pass the threshold for FDR. Selected HIF-1 target genes in the volcano plot (PDK1, GLUT1, HK1 and HK2) were validated by RT-qPCR. Values of RT-qPCR validation are presented as the log2 (Fold Change) in ± SD of three biological duplicates (C).

3.3. HIF-1α is elevated and translocated to the nucleus in COX4-1-deficient cells

To gain further insight into the HIF-1α pathway in COX4-1 deficiency we set out to detect the HIF-1α protein in our model system.

Notably HIF-1α is stabilized under hypoxic conditions, that stabilization enabling it to be translocated to the nucleus, where it functions as a transcriptional activator. Previous studies by Fukuda et al. [18 Fukuda] and others showed that reduced levels of oxygen lead to the elevation of COX4-2 expression. Moreover, they claimed that COX4-2, but not COX4-1, mRNA expression levels were elevated when the cells were treated with the hypoxia inducer, cobalt chloride [18 Fukuda, 19 Hervouet]. In order to understand whether HIF-1 plays a role in the COX4 isoform switch in COX4-1 deficient cells grown under normoxic conditions, we initially analyzed the presence of HIF-1α in whole-cell extracts by immunoblot analysis (Western blot) showing that indeed the level of HIF-1α in HFF-shCOX4I1 cell and patient's cells lysates is markedly elevated (x3.5 and x30 times, respectively) when normalized to beta-Actin, relative to controls (Fig. 4-A,B). To validate HIF-1α activation and band migration, we added cobalt 24hr before performing the assay.

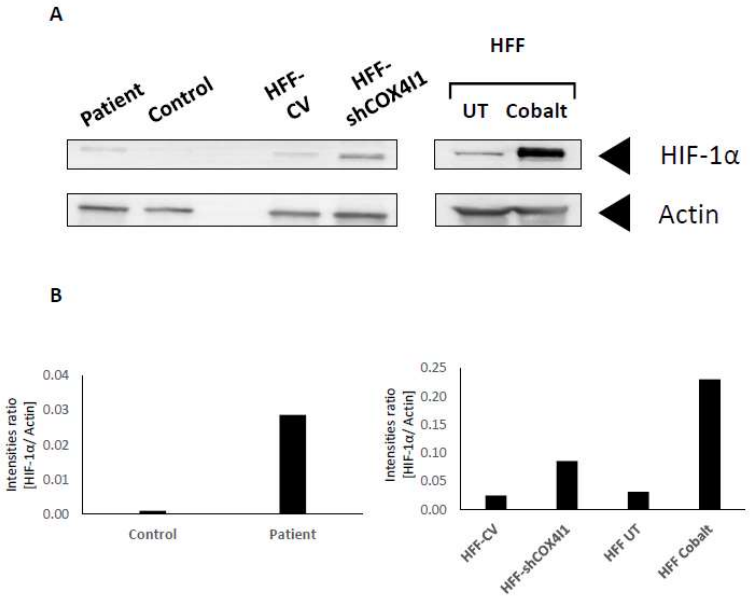

Figure 4. Increased levels HIF-1α in COX4-1-deficient cells. Western blot analysis was performed on cell extracts from both COX4-1-deficient cells (patient and HFF-shCOX4I1), from both corresponding controls. The extracted cells were probed with anti-HIF-1α and anti-actin antibodies as loading control. As a positive control for HIF1-α, untreated (UT) human foreskin fibroblasts (HFF) were preincubated with Cobalt chloride to simulate hypoxia (A). The histogram represents the results normalized to actin

(B). The figure depicts one representative experiment out of three, showing an increased level of HIF-1α in COX4-1 deficient cells.

In order to confirm the presence of HIF-1α and study its cellular localization we co-immunostained HIF-1α with COX4-2 and counter stained with Hoechst-33342. As depicted in Figure 5, COX4-1-deficient cells displayed increased levels of HIF-1α localized in their nuclei, indicating that the elevated levels of HIF-1α, is most probably due to its stabilization. Notably all COX4-2 positive cells showed nuclear HIF-1α stain. The accumulation and translocation of HIF-1α to the nucleus indicate that HIF-1 is activated and thereby inducing the HIF-1 signaling pathway. These results affirm the CEL-Seq2 data analysis (Figure 3A), and verify the regulation of COX4-2 by HIF-1α.

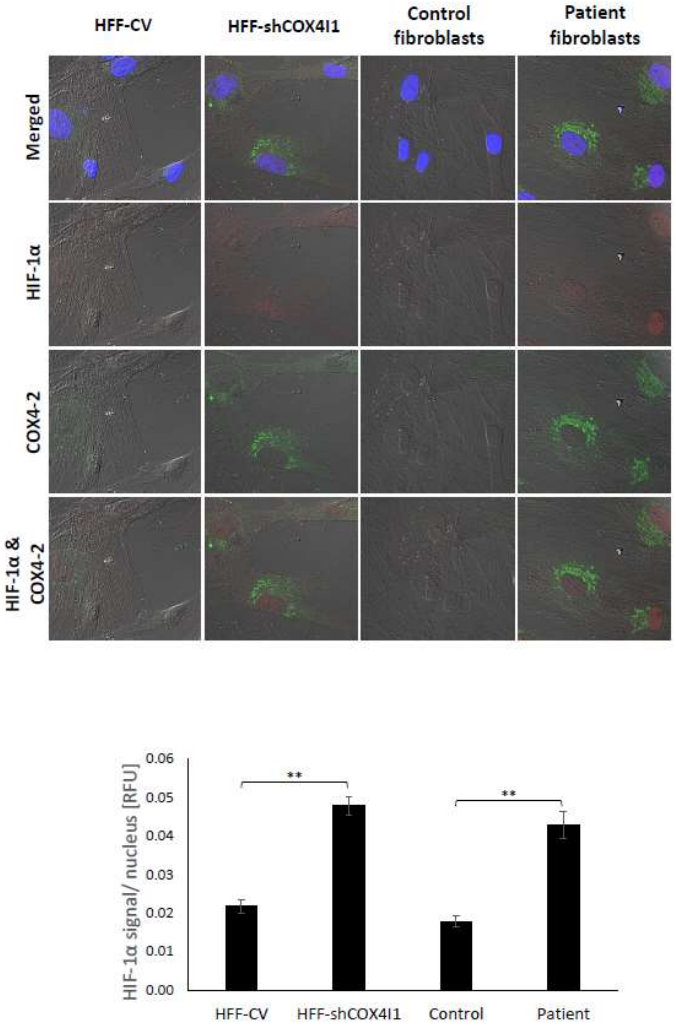

Figure 5. HIF-1α nuclear accumulation is present in COX4-2-positive cells. COX4-1-deficient (HFF-shCOX4I1 and patient) and control cells were stained with antibodies against HIF-1α (red) and COX4-2 (green). Nuclei were visualized by Hoechst-3334. The results demonstrate increased nuclear localization of HIF-1α in COX4-1-deficient cells relative to controls. The observed accumulation of HIF-1α is correlated with COX4-2-positive cells (upper panel). The micrographs were quantified and depicted as histograms of HIF-1α (lower panel) relative signal intensity per nucleus ± SEM of at least 100 nuclei **p<0.01(B).

Nevertheless, we were still puzzled by the fact that upregulation of COX4-2 and HIF-1α occurs under normoxic conditions in our system. Thus, we aimed to strengthen our hypothesis that the upregulation of COX4-2 via HIF-1α occurs also in normoxia. To this

end, we compared the levels of double stained COX4-2 and HIF-1α in untreated cells and in cells treated with cobalt, in order to mimic hypoxia inducing a chemical upregulation of COX4-2. As depicted in Figure 6 A-B, 6 hr of pre-incubation with cobalt led to HIF-1α stabilization (accumulation of HIF-1α in the nuclei) in each type of cell line (both COX4-1-deficient cells and corresponding controls). Interestingly, while a significant increase in the levels of COX4-2 was observed in the controls, COX4-1-deficient cells showed comparable levels of COX4-2, with and without cobalt With respect to nuclear accumulation of HIF-1α, a significant increase was evident upon cobalt treatment in all cells, also in COX4-1-deficient cells. Taking together, we suggest that the levels of COX4-2 in COX4-1-deficient cells are already *a priori* elevated to a maximum at relatively low levels of HIF-1α (compared to cobalt) (Fig. 6B).

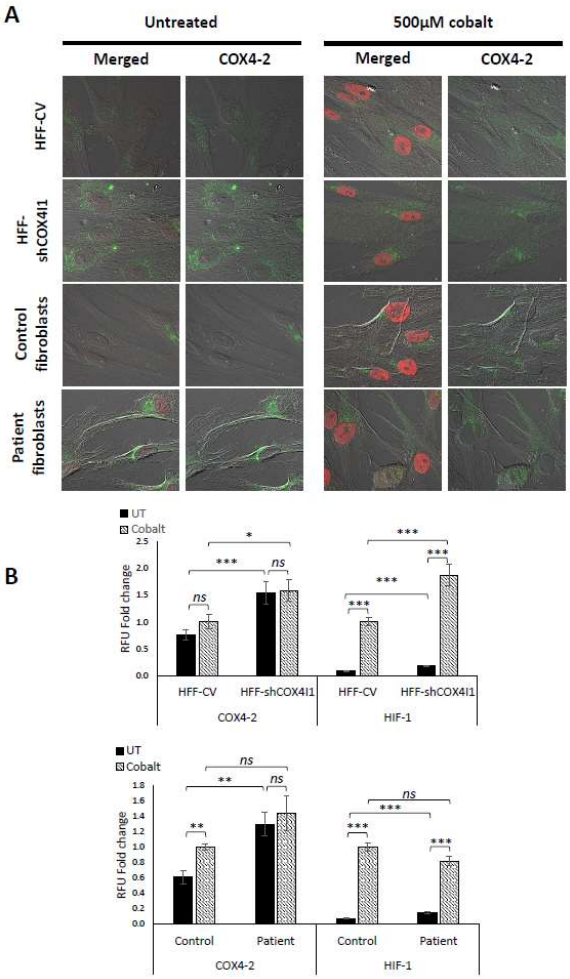

Figure 6. Chemical activation of HIF-1α increase COX4-2 expression in control cells, whereas in COX4-1 deficient cells, the levels remain unchanged. COX4-1-deficient (HFF-shCOX4I1 and patient) and control cells have been either preincubated with or without cobalt for 6 hr prior performing co-staining of COX4-2 and HIF-1α (A). The stabilization of HIF-1α is demonstrated by its translocation to the nuclei of each treated cell. COX4-1-deficient cells did not show any difference in COX4-2 levels with and without cobalt treatment, while nuclear accumulation of HIF-1α was increased (A). The quantified results are depicted in the histogram (B). Values are normalized to the corresponding cobalt-treated control. mean± SEM of at least 70 cells; **p<0.002 compared to corresponding control.

4. Discussion

In this work we show that COX4-1 deficiency due to K101N variant still retains a significant amount of OXPHOS capacity in patients' fibroblasts. This was also confirmed in normal fibroblasts where COX4-1 was downregulated by shRNA. We chose downregulation in fibroblasts over knockdown knockout since it more accurately simulates the phenotype of the patient, which is much milder than other nuclear-encoded isolated COX deficiencies [6-9]. The only mild decrease in both the basal and ATP-linked OCR in COX4-1 knockdown cell line together with comparable levels of ATP-linked OCR in patients' and control fibroblasts, are in accord with our previous result, showing relatively normal ATP production by the luciferin-luciferase assay in the patient' cells [20 Douiev]. These results suggest a cellular compensatory mechanism, in which in order to compensate COX4-1 deficiency, by upregulates the expression of COX4-2. Indeed, we detected an upregulation of the second isoform COX4-2, which likely is the cause of the observed partial rescued phenotype of COX4-1-deficient cells. Since we demonstrated similar results in both the patient's and the COX4-1 knockdown cells, we suggest that this phenomenon is not attributed solely to the K101N variant. Our results are in accord with previously published data obtained in various cell lines [17-19]. Recently, Reguera *et al*, studied each COX4 isoform separately by constructing HEK293-based cell lines with Cas9-mediated COX4 isoforms knockout, followed by stable knock-in of either isoform. In their study, the researchers confirmed different COX kinetics depending which isoform (either COX4-1 or COX4-2) is expressed [21 Reguera 2020]. We also confirmed this, as COX activity in patient's fibroblast mitochondria was not inhibited by ATP, a feature of COX4-2. This in accord with published data showing that the allosteric ATP binding site in COX4-1 is dependent on phosphorylation of S58, while this regulatory residue does not exist in COX4-2 [22 Acin-Peres 2011]. Regretfully we could not perform more in-depth kinetic studies in the HFF-shCOX4I1 cells due impaired growth and chromosomal instability which was more pronounced than in the patient' cells [20], hindering growth, and preventing mitochondrial isolation [manuscript in preparation]. Interestingly, in a reciprocal manner, we previously observed a compensatory upregulation of COX4-1 in COX 4-2 deficiency [10 Steyer]

In order to elucidate a possible pathway through which the upregulation of COX4-2 occurs, we performed RNA-seq analysis (CEL-Seq2) and analyzed the differential gene expression between HFF-shCOX4I1 and control cells, with the same nuclear background. The data was then analyzed by GSEA (Gene Set Enrichment Analysis) in order to detect up and down regulated gene sets. Using this method, we showed that COX4-1 deficiency is accompanied by upregulation of the hypoxia and glycolysis pathways. In order to affirm these results, we analyzed HIF-1α abundance and localization and also verified the upregulation of several HIF-1 target genes. Interestingly, HIF-1α was present in the nucleus under normoxia and without any obvious oxidative stress (ROS were not relatively elevated in both patient's cells [20] and in the knockdown cell lines (results not shown)). Notably, under hypoxia HIF-1α together with HIF-1β form a stabilized HIF-1 complex which acts a transcription factor of a variety of genes that contain the hypoxia response elements; including the *COX4I2* gene [18 Fukuda. Cell (2007)]. There is an evidence that mitochondrial signals, other than hypoxia and ROS, such a redox status (NADH/NAD ratio), metabolites (TCA-intermediate oncometabolites- such as fumarate, succinate, and lactate) and other non-canonical mechanisms, can imitate and evoke hypoxia-like responses and modulate metabolism [reviewed in [23 McElroy and 24 Lomarin]. Interestingly, HIF-1α also induces genetic instability indicating that the regulation of DNA repair is an integral part of the hypoxic response [25 Koshij]. These evidences are in accordance with our previous publications regarding elevated levels of double-stranded breaks (DSBs) and genomic instability in COX4-1-deficient cells. [5,20]. Our results contribute to the elucidation of the role of COX4-1 in metabolism and to the current

understanding of the pathomechanism of COX deficiency due to nuclear-encoded subunits [26 Cutanova]

To conclude, COX4-2 is upregulated and partially rescues COX4-1 deficiency through HIF-1α activation induced by a yet to be characterized, non-canonical pathway.

Acknowledgements
This work was supported by the ISRAELI SCIENCE FOUNDATION (grant #1059/19). The authors declare no conflict of interest. Tal Katz-Ezov Technion Genome Center Haifa is acknowledged for CEL-Seq2 analysis. Dr Sharona Elagvish from Info-CORE, I-CORE Bioinformatics Unit of the Hebrew University of Jerusalem and Hadassah Medical Center, Dr. Michael Berger and Prof. Michal Horowitz Faculty of Medicine Hebrew University of Jerusalem are acknowledged for fruitful discussions.

Author contributions
Conceptualization and Investigation, Liza Douiev, and Ann Saada; Funding acquisition, Ann Saada; Methodology and Interpretation; Liza Douiev, Chaya Miller, Shmuel Ruppo, Hadar Benyamini, Bassam Abu-Libdeh, Ann Saada; Project administration and Supervision, Ann Saada; Writing original draft, Liza Douiev

References

1. Arnold S. The power of life--cytochrome c oxidase takes center stage in metabolic control, cell signalling and survival. Mitochondrion. 2012 Jan;12(1):46-56. doi: 10.1016/j.mito.2011.05.003. Epub 2011 May 26. PMID: 21640202.

2. Sinkler CA, Kalpage H, Shay J, Lee I, Malek MH, Grossman LI, Hüttemann M. Tissue- and Condition-Specific Isoforms of Mammalian Cytochrome c Oxidase Subunits: From Function to Human Disease. Oxid Med Cell Longev. 2017;2017:1534056. doi: 10.1155/2017/1534056. Epub 2017 May 16. PMID: 28593021; PMCID: PMC5448071.

3. Timón-Gómez A, Bartley-Dier EL, Fontanesi F, Barrientos A. HIGD-Driven Regulation of Cytochrome c Oxidase Biogenesis and Function. Cells. 2020 Dec 6;9(12):2620. doi: 10.3390/cells9122620. PMID: 33291261; PMCID: PMC7762129.

4. Abu-Libdeh B, Douiev L, Amro S, Shahrour M, Ta-Shma A, Miller C, Elpeleg O, Saada A. Mutation in the COX4I1 gene is associated with short stature, poor weight gain and increased chromosomal breaks, simulating Fanconi anemia. Eur J Hum Genet. 2017 Oct;25(10):1142-1146. doi: 10.1038/ejhg.2017.112. Epub 2017 Aug 2. PMID: 28766551; PMCID: PMC5602013.

5. Douiev L, Abu-Libdeh B, Saada A. Cytochrome c oxidase deficiency, oxidative stress, possible antioxidant therapy and link to nuclear DNA damage. Eur J Hum Genet. 2018 Apr;26(4):579-581. doi: 10.1038/s41431-017-0047-5. Epub 2018 Feb 2. PMID: 29396562; PMCID: PMC5891488.

6. Pillai NR, AlDhaheri NS, Ghosh R, Lim J, Streff H, Nayak A, Graham BH, Hanchard NA, Elsea SH, Scaglia F. Biallelic variants in COX4I1 associated with a novel phenotype resembling Leigh syndrome with developmental regression, intellectual disability, and seizures. Am J Med Genet A. 2019 Oct;179(10):2138-2143. doi: 10.1002/ajmg.a.61288. Epub 2019 Jul 10. PMID: 31290619.

7. Rak M, Bénit P, Chrétien D, Bouchereau J, Schiff M, El-Khoury R, Tzagoloff A, Rustin P. Mitochondrial cytochrome c oxidase deficiency. Clin Sci (Lond). 2016 Mar;130(6):393-407. doi: 10.1042/CS20150707. PMID: 26846578; PMCID: PMC4948581.

8. Shoubridge EA. Cytochrome c oxidase deficiency. Am J Med Genet. 2001 Spring;106(1):46-52. doi: 10.1002/ajmg.1378. PMID: 11579424.

9. Hock DH, Robinson DRL, Stroud DA. Blackout in the powerhouse: clinical phenotypes associated with defects in the assembly of OXPHOS complexes and the mitoribosome. Biochem J. 2020 Nov 13;477(21):4085-4132. doi: 10.1042/BCJ20190767. PMID: 33151299; PMCID: PMC7657662.

10. Shteyer E, Saada A, Shaag A, Al-Hijawi FA, Kidess R, Revel-Vilk S, Elpeleg O. Exocrine pancreatic insufficiency, dyserythropoeitic anemia, and calvarial hyperostosis are caused by a mutation in the COX4I2 gene. Am J Hum Genet. 2009 Mar;84(3):412-7. doi: 10.1016/j.ajhg.2009.02.006. Epub 2009 Mar 5. PMID: 19268275; PMCID: PMC2668012

11. Golubitzky A, Dan P, Weissman S, Link G, Wikstrom JD, Saada A. Screening for active small molecules in mitochondrial complex I deficient patient's fibroblasts, reveals AICAR as the most beneficial compound. PLoS One. 2011;6(10):e26883. doi: 10.1371/journal.pone.0026883. Epub 2011 Oct 26. PMID: 22046392; PMCID: PMC3202581.

12. Hashimshony T, Senderovich N, Avital G, Klochendler A, de Leeuw Y, Anavy L, Gennert D, Li S, Livak KJ, Rozenblatt-Rosen O, Dor Y, Regev A, Yanai I. CEL-Seq2: sensitive highly-multiplexed single-cell RNA-Seq. Genome Biol. 2016 Apr 28;17:77. doi: 10.1186/s13059-016-0938-8. PMID: 27121950; PMCID: PMC4848782.

13. Marcel M. Cutadapt removes adapter sequences from high-throughput sequencing reads. EMBnet.journal 2011, 17.1:10-12. doi:10.14806/ej.17.1.200

14. Anders S, Pyl PT, Huber W. HTSeq--a Python framework to work with high-throughput sequencing data. Bioinformatics. 2015 Jan 15;31(2):166-9. doi: 10.1093/bioinformatics/btu638. Epub 2014 Sep 25. PMID: 25260700; PMCID: PMC4287950.

15. Arnold S, Kadenbach B. Cell respiration is controlled by ATP, an allosteric inhibitor of cytochrome-c oxidase. Eur J Biochem. 1997 Oct 1;249(1):350-4. doi: 10.1111/j.1432-1033.1997.t01-1-00350.x. PMID: 9363790.

16. Aras S, Pak O, Sommer N, Finley R Jr, Hüttemann M, Weissmann N, Grossman LI. Oxygen-dependent expression of cytochrome c oxidase subunit 4-2 gene expression is mediated by transcription factors RBPJ, CXXC5 and CHCHD2. Nucleic Acids Res. 2013 Feb 1;41(4):2255-66. doi: 10.1093/nar/gks1454. Epub 2013 Jan 8. PMID: 23303788; PMCID: PMC3575822.

17. Tam SY, Wu VWC, Law HKW. Hypoxia-Induced Epithelial-Mesenchymal Transition in Cancers: HIF-1α and Beyond. Front Oncol. 2020 Apr 8;10:486. doi: 10.3389/fonc.2020.00486. PMID: 32322559; PMCID: PMC7156534.

18. Fukuda R, Zhang H, Kim JW, Shimoda L, Dang CV, Semenza GL. HIF-1 regulates cytochrome oxidase subunits to optimize efficiency of respiration in hypoxic cells. Cell. 2007 Apr 6;129(1):111-22. doi: 10.1016/j.cell.2007.01.047. PMID: 17418790.

19. Hervouet E, Pecina P, Demont J, Vojtísková A, Simonnet H, Houstek J, Godinot C. Inhibition of cytochrome c oxidase subunit 4 precursor processing by the hypoxia mimic cobalt chloride. Biochem Biophys Res Commun. 2006 Jun 16;344(4):1086-93. doi: 10.1016/j.bbrc.2006.04.014. Epub 2006 Apr 19. PMID: 16643849.

20. Douiev L, Saada A. The pathomechanism of cytochrome c oxidase deficiency includes nuclear DNA damage. Biochim Biophys Acta Bioenerg. 2018 Sep;1859(9):893-900. doi: 10.1016/j.bbabio.2018.06.004. Epub 2018 Jun 7. PMID: 29886046.

21. Pajuelo Reguera D, Čunátová K, Vrbacký M, Pecinová A, Houštěk J, Mráček T, Pecina P. Cytochrome c Oxidase Subunit 4 Isoform Exchange Results in Modulation of Oxygen Affinity. Cells. 2020 Feb 14;9(2):443. doi: 10.3390/cells9020443. PMID: 32075102; PMCID: PMC7072730.

22. Acin-Perez R, Gatti DL, Bai Y, Manfredi G. Protein phosphorylation and prevention of cytochrome oxidase inhibition by ATP: coupled mechanisms of energy metabolism regulation. Cell Metab. 2011 Jun 8;13(6):712-9. doi: 10.1016/j.cmet.2011.03.024. PMID: 21641552; PMCID: PMC3118639.

23. McElroy GS, Chandel NS. Mitochondria control acute and chronic responses to hypoxia. Exp Cell Res. 2017 Jul 15;356(2):217-222. doi: 10.1016/j.yexcr.2017.03.034. Epub 2017 Mar 19. PMID: 28327410; PMCID: PMC5474758.

24. Iommarini L, Porcelli AM, Gasparre G, Kurelac I. Non-Canonical Mechanisms Regulating Hypoxia-Inducible Factor 1 Alpha in Cancer. Front Oncol. 2017 Nov 27;7:286. doi: 10.3389/fonc.2017.00286. PMID: 29230384; PMCID: PMC5711814.

25. Koshiji M, To KK, Hammer S, Kumamoto K, Harris AL, Modrich P, Huang LE. HIF-1alpha induces genetic instability by transcriptionally downregulating MutSalpha expression. Mol Cell. 2005 Mar 18;17(6):793-803. doi: 10.1016/j.molcel.2005.02.015. PMID: 15780936.

26. Čunátová K, Reguera DP, Houštěk J, Mráček T, Pecina P. Role of cytochrome c oxidase nuclear-encoded subunits in health and disease. Physiol Res. 2020 Dec 22;69(6):947-965. doi: 10.33549/physiolres.934446. Epub 2020 Nov 2. PMID: 33129245.